Structural Eng. / Earthquake Eng. Vol. 5. No. 2, 343s-350s. October 1988
Japan Society of Civil Engineers (Proc. of JSCE No. 398/I-10)

EFFECTS OF CYCLIC LOADING HYSTERESIS ON DYNAMIC BEHAVIOR OF REINFORCED CONCRETE BRIDGE PIERS

By Kazuhiko KAWASHIMA and Tatsuhiko KOYAMA***

A series of dynamic loading tests with use of large-scale reinforced concrete bridge piers were conducted to investigate an effect of loading hysteresis under displacement control load reversal tests. The specimens were subjected to three loading hysteresis which idealized sequence of loading displacement developed during earthquakes, i. e., in Type 1 loading, displacement was monotonically increased with increasing number of load reversals, and Type 2 used a hysteresis in the reversal order of the Type 1. Type 3 loading used a combination of Type 1 and Type 2 loading.

It was understood from the study that energy dissipation capabilities depend on the loading hysteresis. First large displacement progresses deterioration of energy absorbing capability. It was also found that skelton curve of the hysteresis loop shows significant differences in accordance with loading path.

Keywords : loading test, ductility, seismic design, reinforced concrete column

1. INTRODUCTION

Various studies have been conducted to investigate inelastic behavior of reinforced concrete bridge piers subjected to significant earthquake ground motions, and specimens simulating reinforced concrete bridge piers have been tested under various loading conditions such as static and dynamic cyclic loading, and earthquake-like loading[1)~5)]. In almost all the tests, however, loads were step-wise increased monotonically up to failure, in which at each time step several cycles of symmetrical loading reversals with the same displacement amplitude were carried out. Although loading hysteresis has a significant effect on the test results, little is known about the effect of loading hysteresis on the mechanism of inelastic behavior of reinforced concrete bridge piers.

Because the structural response of bridges results in various loading hysteresis in the piers, it is inevitable to study such effects in order to apply the dynamic loading test data for practical seismic design of reinforced concrete bridge piers.

This study presents a series of dynamic loading test results of large-size reinforced concrete bridge pier models subjected to different loading hysteresis. Effect of loading hysteresis on strength and energy dissipating capacity is presented.

2. TEST SPECIMENS AND EXPERIMENTAL SET-UP

Five large-size reinforced concrete specimens simulating cantilever piers of bridges as shown in Fig. 1 were used for the test. The cantilever pier was framed into a massive reinforced concrete footing which

* Member of JSCE, Dr. Engr., Head of Earthquake Engineering Division, Earthquake Disaster Prevention Department, Public Works Research Institute, Ministry of Construction (Tsukuba Science City, Ibaraki-ken, Japan)
** Member of JSCE, Assistant Research Engineer, ditto.

was anchored to a test floor by means of post tensioned rods.

Five specimens have the same characteristics over the cross section of 80×40 cm, effective height h, which is designated as a distance from bottom to the center of loading point, of 240 cm, main reinforcement ratio of 0.87 % with use of 11 SD30 bars (deformed bars) with diameter of 13 mm, and tie reinforcement ratio of 0.08 % with use of 9 mm diameter SR24 bars (plain bar) placed at 20 cm intervals. Shear span ratio h/d, which is defined as a ratio between effective height h and effective width d (width substituted by covering depth), is 6.8. It should be noted that the main reinforcements were placed only at two sides which are subjected to tension and/or compression due to load reversals, i.e., no main reinforcements were placed at the other two sides parallel to loading direction because determination of yield displacement is much easier by disregarding them. The layout of tie bars depends on the Japanese practice in accordance with the Specifications for Design of Highway Bridges[6]. The tie bars were lapped at least 60 mm. They used portland cement with uni-axial compression strength ranging from 368 to 448 kgf/cm^2, and aggregates with the maximum grain size of 10 mm.

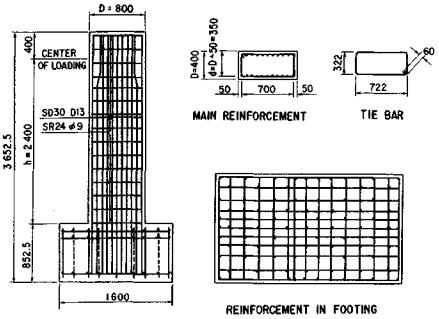

Fig. 1 Test Specimens.

Two specimens were used for each of Type 2 and Type 3 loadings, which will be described later, and one specimen for Type 1 loading. They are designated as P-40 (Type 1 loading), P-41 and P-42 (Type 2 loading), and P-43 and P-44 (Type 3 loading), which represent a sequential number to identify specimens tested at the Public Works Research Institute.

3. LOADING CONDITION

The specimens were loaded at the cantilever tip as shown in Fig. 2 by means of an electro-hydlaulic dynamic actuator with max. loading velocity of 1m/sec. Although a compressive stress of 5 to 20 kgf/cm^2 is generated in piers with ordinary shape and height due to weight of superstructure, it was disregarded in the test because it was considered that such a small stress results in limited influence for effects of loading hysteresis.

The specimens were subjected to a series of symmetrical load reversals with three different hystereses as shown in Fig. 3, i.e., in Type 1 loading, displacement was monotonically increased with increasing number of load reversals, and Type 2 used a hysteresis in the reversal order of the Type 1. Type 3 loading used combination of Type 1 and Type 2 loading.

Total number of load reversals and the maximum displacement were determined as twenty and displacement ductility factor of ten, respectively, over the three types of loading. The yield displacement δ_y corresponding to one displacement ductility factor was defined as the displacement at loading point at which reinforcing bars of the extreme tension fiber at the bottom of cantilever specimen reached yield

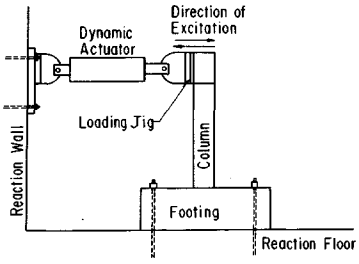

Fig. 2 Experimental Set-up.

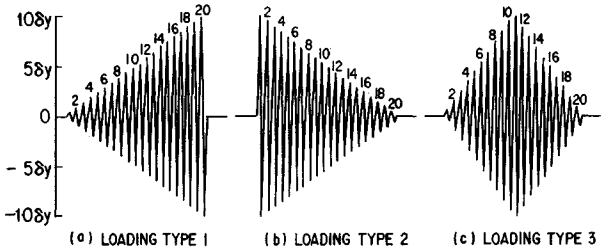

Fig. 3 Hysteresis of Loading Displacement.

strain. The yield strain of reinforcement was assumed as 1 800 μ based on a number of tensile test of the specimens. The step-size for either increasing or decreasing the loading displacement in each step was assumed as displacement ductility factor of 0.5 for Type 1 and Type 2 loadings, and 1.0 for Type 3 loading, respectively. It should be noted, however, that in Type 3 loading, loading displacement was increased as 0.5 δ_y, 1.5 δ_y, 2.5 δ_y, ……, 9.5 δ_y and 10 δ_y while it was decreased as 9 δ_y, 8 δ_y, …… 2 δ_y, 1 δ_y so that accumulated displacement amplitude during total load reversals be the same over the three loading hystereses. Type 3 loading has two loading steps, i.e., hysteresis in which displacement is increased and that in which displacement is decreased. To identify the two stages, they are designated hereinafter as an increasing path and a decreasing path, respectively.

Although the loading pattern was significantly simplified, it was anticipated that loading hysteresis of Type 3 represents typical ground motion induced by earthquakes. In comparison, since ground acceleration developed by earthquakes with moderate magnitude and short epicentral distance tends to increase rapidly in time[7], loading hysteresis of Type 2 may be regarded as that developed by such earthquakes. It should be noted that even in the moderate earthquake, the ground intensity is sometimes large enough to develop 10 δ_y displacement in the reinforced concrete bridge piers as was observed during the Miyagi-ken-oki earthquake of 1978. Loading hysteresis of Type 1 is a standard hysteresis which has been commonly adopted in the most of past loading tests. Loading velocity was taken as 2.4 mm/sec over each step in all the three loading hystereses.

4. EFFECT OF LOADING HYSTERESIS

(1) Failure mode

Figs. 4, 5 and 6 show failure modes of the model piers with emphasis on cracks and spalling-off of cover concrete as well as elongation of reinforcements. Failure modes on the side subjected to tension and compression are presented here so that progress of failure mode be clearly observed. Although two specimens were used for Type 2 and Type 3 loadings to check differences between specimens, only the results of one of the two specimens are presented in Figs. 5 and 6 because the failure modes of the two specimens are of the same type. All the specimens failed in flexure at their foots.

In the specimen subjected to Type 1 loading, flexural cracks were gradually formed at the base of column in accordance with increase of loading displacement. Significant flexural cracks and spalling-off of cover concrete at the region of 20 cm from the bottom were developed during load reversals with 7 δ_y and 8 δ_y, respectively. Inelastic buckling of main reinforcements either outwards between two adjacent tie bars or sideways were progressively developed. Cut of main reinforcement was not, however, developed.

On the other hand, in the specimen subjected to Type 2 loading, flexural cracks were formed at the extreme tension fiber (④ side) on the way to 10 δ_y loading while any significant failure was not observed at the compression side (② side). Crack developed at 20 cm from the bottom, where the lowest tie reinforcement was placed, was the most significant among several flexural cracks at the tension side, and it had a width of more than 5 mm at 8 δ_y loading (refer to Fig. 5(c)). After unloading from 10 δ_y displacement, on the way to -10 δ_y loading, flexural cracks were formed at the tension side (② side), as was developed at the tension side (④ side) on the loading to the first 10 δ_y. However, progress of failure of cover concrete at the compression side (④ side), which was developed by the previous loading to 10 δ_y by flexure, did not occur. Spalling-off of cover concrete and outward buckling of main reinforcements were initiated on the unloading from -10 δ_y, and became significant when loading toward 9.5 δ_y displacement was initiated. After the completion of 9.5 δ_y load reversals, cover concrete almost dropped out up to 40 cm from bottom of the pier (refer to Fig. 5(f)). However, further progress of failure associated with load reversals with 9 δ_y (refer to Fig. 5(g)), 8.5 δ_y, ……, was no longer developed.

In the specimen subjected to Type 3 loading, failure mode developed in the increasing path was essentially the same with that developed in the Type 1 loading, i.e., flexural failure progressed in

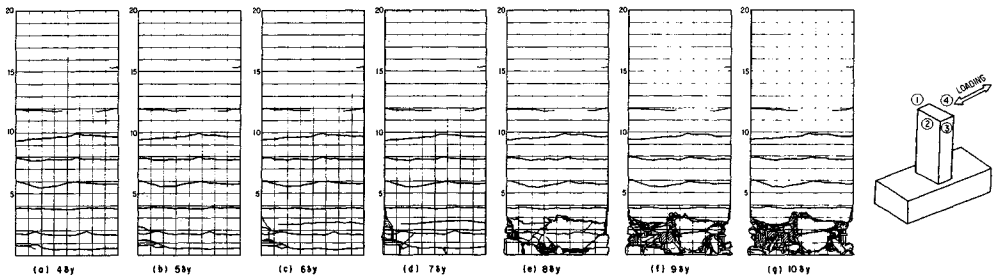

Fig. 4 Failure Mode of P-40 Subjected to Type 1 Loading (④ Side).

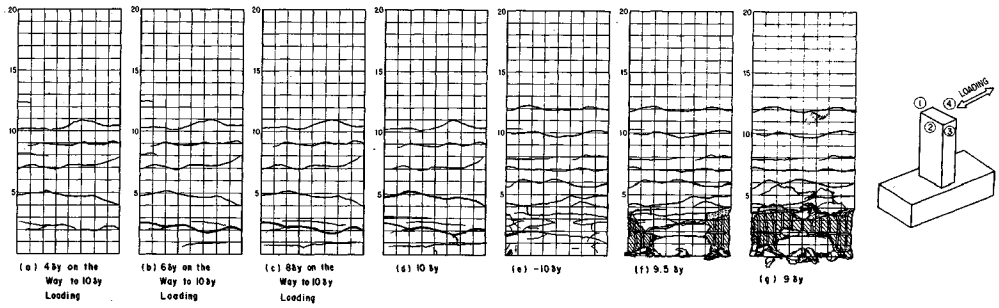

Fig. 5 Failure Mode of P-41 Subjected to Type 2 Loading (a, b, c and d : ④ side, e, f and g : ② side).

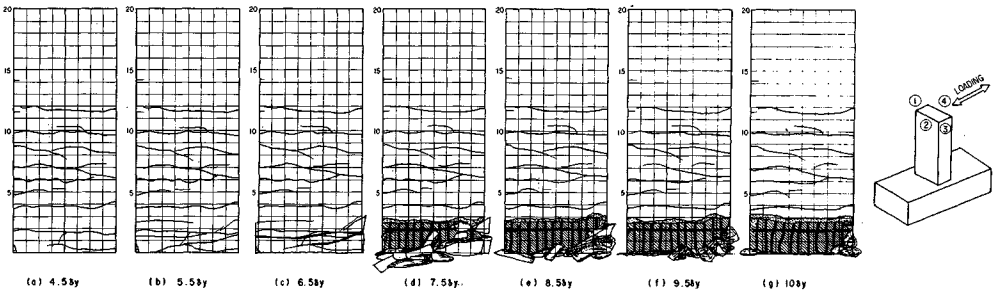

Fig. 6 Failure Mode of P-43 Subjected to Type 3 Loading (④ Side).

accordance with increase of loading displacement, and significant spalling-off of cover concrete and outward buckling of main reinforcement were developed during 6.5 δ_y loading. Failure mode developed in the decreasing path was also similar with that developed in the Type 2 loading.

(2) Strength and deformation capability

Fig. 7 shows continuous plot of hysteresis loop of the load vs. displacement at the loading point for the specimens subjected to three loading patterns. It should be noted in Type 2 loading that because loading was interrupted at the displacement of $\pm\delta_y$, $\pm 2\,\delta_y$, $\pm 3\,\delta_y$, ……, $\pm 10\,\delta_y$ on the loading during first reversal with amplitude of 10 δ_y for approximately ten minutes to observe flexural cracks developed on the surface of specimen, small pulse-like drops in load were developed in the hysteresis loops.

In the specimen subjected to Type 1 loading, force-displacement relation was stable up to loading displacement of 6 δ_y, and significant drop in force was developed at 7 δ_y associated with spalling-off of cover concrete. In comparison, hysteresis loop of the specimen subjected to Type 2 loading was stable from the beginning of first loading toward $+10\,\delta_y$ up to the displacement at which load was reversed to zero after excursion of $-10\,\delta_y$. During these excursion, the hysteresis loop shows parallerogram shape which implies that energy dissipation capability is quite large. However the load after completion of first cycle of load reversal was only about 4 tf, which is approximately 40 % of the maximum load. This implies that

significant decrease of restoring force was developed during unloading from $-10\,\delta_y$. Hysteresis loop of the specimen subjected to Type 3 loading shows the similar feature with that of Type 1 loading and Type 2 loading in increasing path and decreasing path, respectively.

Fig. 8 shows comparison of hysteresis loops between three loading patterns at loading displacement of $2.5\,\delta_y$, $5.5\,\delta_y$ and $8.5\,\delta_y$. It should be noted in Fig. 8 that in the hystereses of decreasing path of Type 3 loading, hysteresis loops with loading displacement of $2\,\delta_y$, $5\,\delta_y$ and $8\,\delta_y$ are presented instead of $2.5\,\delta_y$, $5.5\,\delta_y$ and $8.5\,\delta_y$, respectively, because of the step size of loading displacement described in the preceding section. It is seen from these comparisons that the hysteresis loops at $2.5\,\delta_y$ and $5.5\,\delta_y$ are almost identical between Type 1 loading and Type 3 loading on increasing path, and the same features are observed in the hysteresis loops between Type 2 and Type 3 loading on decreasing path. Of particular importance is the difference of hysteresis loop of Type 3 loading between increasing path and decreasing path, i.e., the hysteresis loop is very much different whether the specimen has already experienced the largest loading displacement or not. This clearly shows the importance to take account of loading hysteresis. Although coincidence of hysteresis loops at $8.5\,\delta_y$ between three loading types is rather poor as compared with those observed at $2.5\,\delta_y$ and $5.5\,\delta_y$ since large loading displacement resulted in significant deterioration of the specimen, the same tendency described above, however, can still be observed. It is interesting to note that lateral load corresponding to the same displacement amplitude is smaller in those specimens subjected to larger number of loading reversals. Fig. 9 shows skeleton curves of hysteresis loop and compares them between three loading patterns. Although the load dropped in Type 1 at $6\,\delta_y$, excluding such a drop of Type 1 loading, the skeleton curves on increasing path and that of decreasing path of Type 3 loading are very much similar with those of Type 1 and Type 2, respectively.

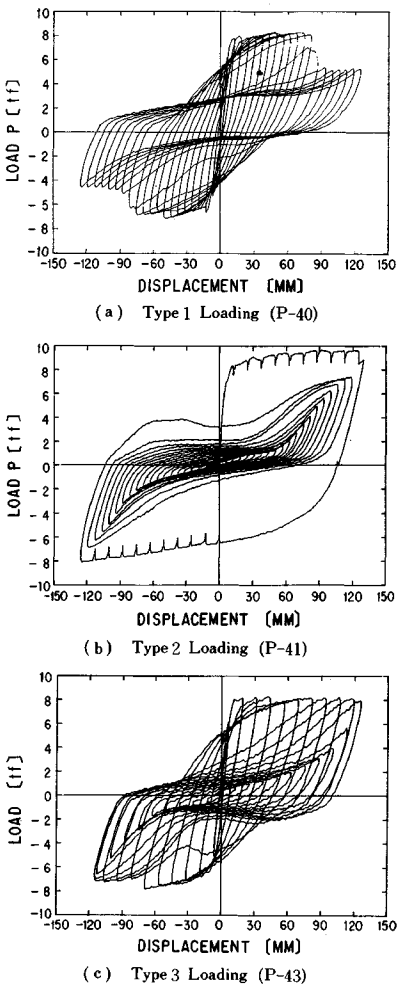

Fig. 7 Hysteresis Loops of Force vs. Displacement.

(3) Equivalent stiffness

As was discussed in the preceding section, stiffness of the specimen shows significant differences

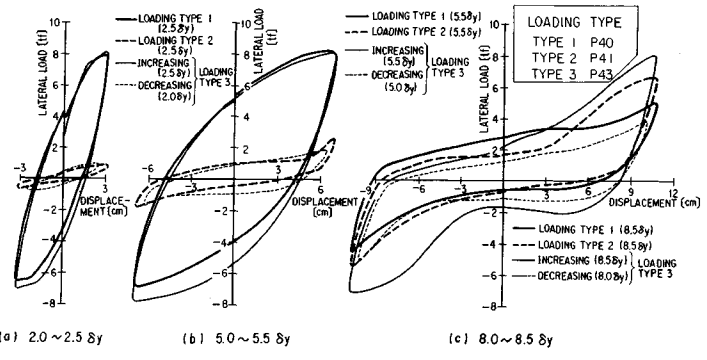

Fig. 8 Comparison of Hysteresis Loops at Loading Displacement of $2.5\,\delta_y$, $5.5\,\delta_y$ and $8.5\,\delta_y$.

between before and after the peak loading displacement. Therefore, an equivalent stiffness K_e was defined as shown in Fig. 10, i. e., secant stiffness connecting two points on hysteresis loop at which maximum loading displacement was developed. It should be noted that the equivalent stiffness thus defined is an important factor representing instantaneous natural period of specimen subjected to significant ground motions.

Fig. 11 shows variation of the equivalent stiffness K_e vs. loading displacement relation for three loading patterns. It is apparent that the equivalent stiffness K_e at increasing path and decreasing path of Type 3 loading is almost identical with that of Type 1 and Type 2 loadings, respectively. It should be noted that on the increasing path, the equivalent stiffness K_e deteriorates significantly in accordance with increase of loading displacement, i. e., the equivalent stiffness K_e at $2\delta_y$ is only about one third of that at δ_y. On the decreasing path, the equivalent stiffness K_e decreases in accordance with decrease of loading displacement, although it is less significant.

(4) Energy absorbing capability

An area surrounded by a hysteresis loop as shown in Fig. 10 represents an amount of energy dissipated during that load reversal, and hence accumulating the energy dissipation during each load reversal, total amount of energy dissipated in the specimen during the loading test may be evaluated. Figs. 12 and 13 represents variation of energy dissipation per loading cycle and accumulation of the dissipated energy, respectively, with respect to increase and/ or decrease of loading displacement.

It is seen in Fig. 12 that in Type 1 loading, the absorbed energy per cycle increases almost linearly with increasing loading displacement and takes a peak value at $6\delta_y$. On the other hand, in Type 2 loading, although large energy was absorbed at the first reversal with $10\delta_y$, it decreases promptly with decreasing the loading displacement. It is also seen in Fig. 13 that the accumulated energy dissipation was largest in Type 1 followed by Type 3, and that the accumulated energy dissipation of Type 2 is approximately 30 % smaller than that of Type 3. This implies that the specimen subjected to large

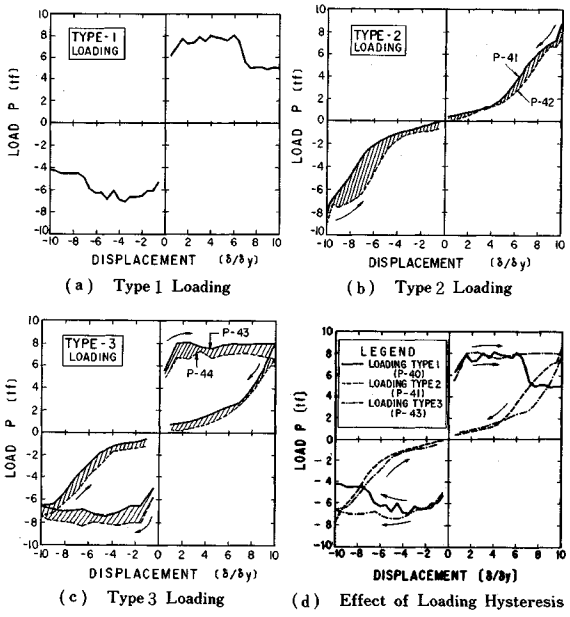

(a) Type 1 Loading (b) Type 2 Loading

(c) Type 3 Loading (d) Effect of Loading Hysteresis

Fig. 9 Skelton Curves of Hysteresis Loop.

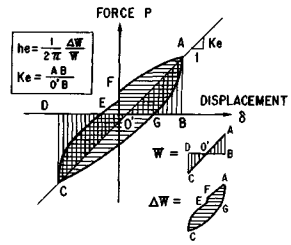

Fig. 10 Definition of Equivalent Stiffness and Equivalent Hysteretic Damping Ratio.

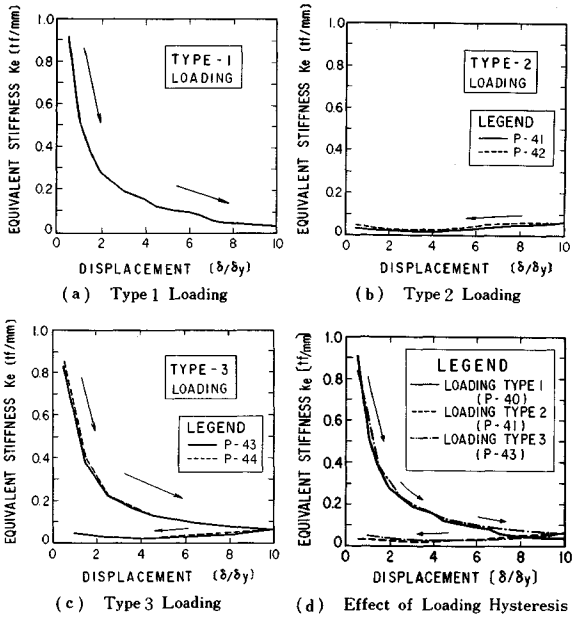

(a) Type 1 Loading (b) Type 2 Loading

(c) Type 3 Loading (d) Effect of Loading Hysteresis

Fig. 11 Equivalent Stiffness K_e.

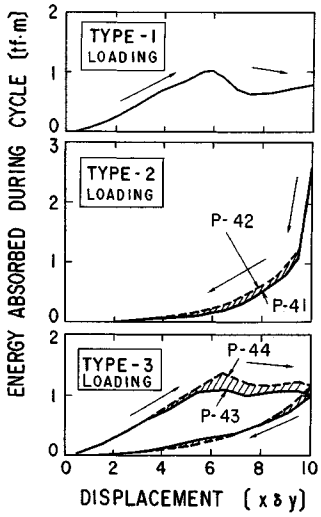

(a) Absorbed Energy ~ Displacement Relation for Each Specimen

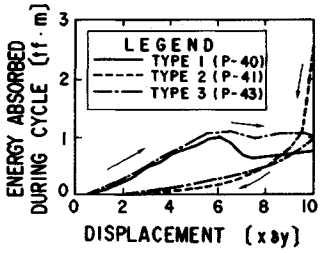

(b) Effect of Loading Hysteresis

Fig. 12 Absorbed Energy per Cycle.

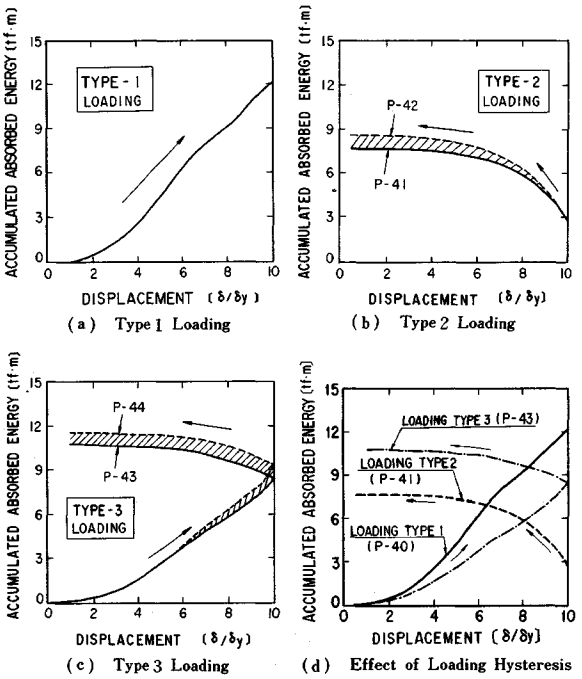

(a) Type 1 Loading (b) Type 2 Loading

(c) Type 3 Loading (d) Effect of Loading Hysteresis

Fig. 13 Accumulated Absorbed Energy.

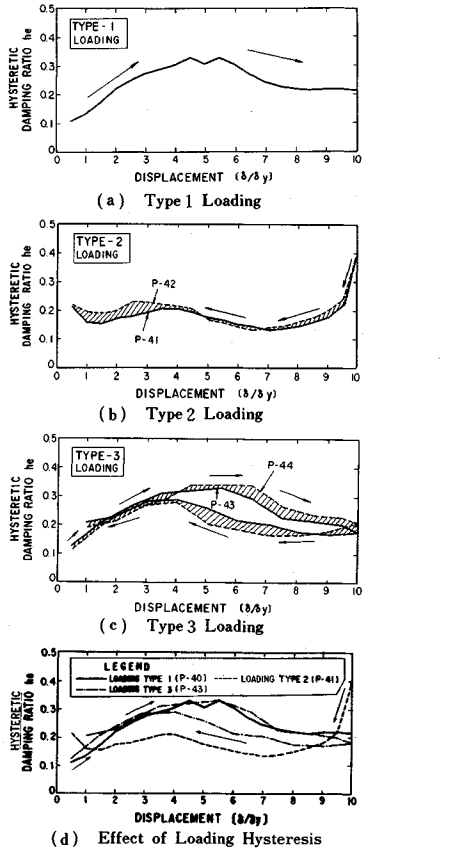

(a) Type 1 Loading

(b) Type 2 Loading

(c) Type 3 Loading

(d) Effect of Loading Hysteresis

Fig. 14 Equivalent Hysteretic Damping Ratio.

loading displacement from the first reversal shows significant deterioration for energy absorbing capacity.

Energy dissipation capacity was also studied in terms of an equivalent hysteretic damping ratio h_e which is defined as

$$h_e=\frac{1}{2\pi}\frac{\Delta W}{W} \quad \cdots\cdots (1)$$

in which ΔW is an energy dissipation during one reversal and W is an elastic energy as defined in Fig. 10.

Fig. 14 shows variation of the hysteretic damping ratio h_e with respect to loading displacement. As a general trend, this relation is closely related with those presented in Fig. 12. The equivalent damping ratio h_e takes a peak value of approximately 0.3 at 4~6 δ_y in Type 1 and Type 3, and becomes smaller with respect to either increase or decrease of loading displacement. The equivalent damping ratio h_e in Type 2 is, however, appreciably smaller at 4~6 δ_y than that of Type 1 and Type 3, although

it takes peak values of 0.4 at 10 δ_y. This may be attributed to quick deterioration of energy absorbing capacity due to first large load reversal.

5. CONCLUDING REMARKS

For aiming to study the effect of loading hysteresis on strength and energy dissipation capability of reinforced concrete bridge piers, a series of dynamic loading tests with use of three different symmetrical loading hystereses with loading velocity of 2.4 mm/sec was conducted over five large-size specimens with shear-span ratio of 6.8, which failed in flexure. Axial force was disregarded here because compressive stress generated in the piers with ordinary shape and height due to weight of superstructure is limited. Based on the test results presented, the following conclusions may be deduced :

(1) Effects of loading hysteresis between Types 1, 2 and 3 are less significant on the maximum load, and equivalent stiffness of the specimens. However, energy dissipation capabilities in terms of accumulated energy dissipation and equivalent hysteretic damping ratio depends on the loading hysteresis, i.e., they are significantly smaller in the specimens subjected to Type 2 loading than those subjected to Type 1 and 3 loadings. First large displacement progressed deterioration of energy absorbing capability of the specimens subjected to Type 2 loading.

(2) Progress of failure which was caused by the previous load reversals is not significantly developed unless the loading displacelent is larger than that of the previous one.

(3) Skeleton curve of the hysteresis loop depends on the loading path, i.e., skeleton curve developed during increasing path is different with that developed during decreasing path. Consequently, prediction of the time at which the peak response displacement is developed is quite important for nonlinear response of reinforced concrete bridge piers.

ACKNOWLEDGMENTS

The authors express their cordial appreciation to Mr. Kinji Hasegawa and Mr. Takeshi Yoshida, member of Earthquake Engineering Division of the Public Works Research Institute, for their efforts and cooperation in performing the dynamic loading tests. The authors also thank to Dr. Toshio Iwasaki for his encouragement throughout this study.

REFERENCES

1) Mahin, S.A. and Bertero, V.V. : Rate of Loading Effects on Uncracked and Repaired Reinforced Concrete Members, EERC Report 72-9, University of California, Berkeley, U.S.A., 1972.
2) Park, R. and Blakeley R.W.G. : Seismic Design of Bridges, RRU Bulletin 43, National Road Board, New Zealand, 1978.
3) Ohta, A. : A study on Earthquake Resistant Design for Reinforced Concrete Bridge Piers of Single-column Type, Report of the Public Works Research Institute, Vol.153, Ministry of Construction, 1980 (in Japanese).
4) Ozaka, Y., Suzuki, M., Kuwasawa, S. and Ishibashi, T. : Load-Deflection Characteristics of Reinforced Concrete Columns Under Static Alternating Cyclic Loads, Proc. of JSCE, Vol.372/V-5, 1986.
5) Cheok, G.S. and Stone, W.G. : Behavior of 1/6-Scale Model Bridge Columns Subjected to Cyclic Inelastic Loading, NBS I 86-3494, National Bureau of Standards, U.S.A., 1986.
6) Japan Road Association : Specifications for Design of Highway Bridges, Part Ⅳ Design of Foundation, 1980.
7) Kawashima, K. and Aizawa, K. : Duration of Strong Motion Acceleration Records, Proc. of JSCE, Vol.2-2, 1985.

(Received August 10 1987)